JOURNAL OF SOLID STATE CHEMISTRY 5, 212–225 (1972)

Electron Microscopy of Solid Solutions and Crystallographic Shear Structures

II. Fe_2O_3–TiO_2 and Ga_2O_3–TiO_2 Systems*

R. M. GIBB AND J. S. ANDERSON

Inorganic Chemistry Laboratory, University of Oxford, Oxford, England

Received October 14, 1971

Replacement of Ti^{4+} in TiO_2 by Fe^{3+} or Ga^{3+} gives a limited range of solid solutions with anion-deficient rutile structure. Anion deficiency is accommodated by eliminating a sheet of O^{2-} sites by a new type of planar boundary, on ⟨210⟩ (rutile), with the extinction characteristics of an α boundary and apparent displacement vector $\frac{1}{2}[0,1,0]$. Structural considerations suggest, however, that this is neither a true α boundary nor a crystallographic shear plane as hitherto defined. In Fe_2O_3–TiO_2 solid solutions, rutile with isolated ⟨210⟩ boundaries coexists with Fe_2TiO_5. In Ga_2O_3–TiO_2, parallel recurrent [210] boundaries generate a new homologous series of phases $Ga_4Ti_{n-4}O_{2n-2}$ ($15 < n < 23$, n odd) which were characterized in an imperfectly ordered state by electron diffraction and direct lattice imaging.

Changes in the anion:cation ratio of ionic crystals can be brought about not only by stoichiometric variability (e.g. through partial reduction) but also by solid solution, through incorporation of cations with similar ionic radius but different ionic charge from the cations of the host structure. In this paper we discuss the structural consequences of introducing M^{3+} cations into the rutile structure of TiO_2.

Rutile-based structures have latterly been intensively studied in order to elucidate the principles of crystallographic shear, which is basically a means of accommodating a change in the anion:cation ratio without gross structural change, localized defects or change of cation coordination. Electron microscopy has proved to be a powerful means of recognizing and interpreting the resultant derivative structures, with their large unit cells, and of determining the imperfection of their internal order. It has, moreover, revealed that the binary oxides, at least, can eliminate localized defects even for very small deviations from the ideal composition. In very slightly substoichiometric TiO_2 and WO_3 the deficit of oxygen is largely accounted for by the formation of isolated crystallographic shear planes as two-dimensional planar faults ('Wadsley defects').

It is now familiar that, in the binary Ti–O system, there are two homologous series of oxides Ti_nO_{2n-1}: those with $4 < n < 10$ based on recurrent shear on the $\{1\bar{2}1\}$ rutile plane (*1–7*) and a second series, revealed only by electron microscopy, in the composition range $TiO_{1.937}$ to $TiO_{1.975}$, ca. $16 < n <$ ca. 40, with $\{1\bar{3}2\}$ crystallographic shear planes (*5, 6, 8, 9*). Random Wadsley defects on all $\{1\bar{3}2\}$ orientations are already present at compositions around $TiO_{1.999}$. These are all mixed valence phases, based formally on Ti^{3+} and Ti^{4+} cations, and it might be surmised that delocalization of electrons, between crystallographically equivalent cations in different charge states, played some part in crystallographic shear. Although this would facilitate the ordering of cations of different valence states, it is clear that facile electron transfer is not essential, since a series of $\{1\bar{2}1\}$ crystallographic shear phases $Cr_2Ti_{n-2}O_{2n-1}$ ($n > 6$) was identified by X-ray diffraction methods in the Cr_2O_3–TiO_2 system (*3, 10*); electron microscopy has shown that this series extends to $n = 11$ (*11*). With decrease in the chromium concentration (i. e., decreasing anion deficit), there is no single change

* Part I: *J. Solid State Chem.* **4**, 379 (1972).

over to a homologous series based on $\{1\bar{3}2\}$ shear; instead, the orientation of the crystallographic shear plane changes progressively and sweeps through a continuous range of $\{h\bar{k}l\}$ values in the $[1\bar{1}1]$ zone, between $\{1\bar{2}1\}$ and $\{1\bar{3}2\}$ (*11*, *12*). Still closer to the rutile composition (from about $MO_{1.99}$ to $MO_{2.00}$, where M = Cr + Ti) there is a solid solution phase in which no $\{1\bar{3}2\}$ boundaries or other Wadsley defects have been found. The conclusion that these are anion-deficient structures, with random localized defects or defect clusters, seems inescapable.

Thus, although other M^{3+} cations can replace Ti^{3+} in rutile-based structures, they may modify the way in which the oxygen deficiency is accommodated. It was therefore of interest to replace Cr^{3+} by other suitable cations, as controllers of the overall stoichiometry, in order to identify the factors that determine the structures assumed in $TiO_2 + MO_{1.5}$ systems. The cations studied should preferably have no ambiguity about their valence state in the as-prepared oxides. They must have ionic radii close to that of Ti^{3+}; small differences in packing radius could have significant effects on the coulombic and repulsive terms of the lattice energy and, more particularly, on the local relaxation and distortion of the crystal structures around the trivalent cations. The electronic configuration of the cations may be important; there is a significant component of covalent binding in the rutile structure and it has been suggested that direct *d–d* interactions could operate between cations in the shear plane where face sharing between coordination octahedra leads to short metal–metal atomic distances. The *d* character and radial extension of the *d* orbitals could therefore be variables influencing the behaviour of ternary oxide systems.

We have accordingly examined a number of systems and report here in some detail our observations on $GaO_{1.5}$–TiO_2 and $FeO_{1.5}$–TiO_2. We find that these introduce a new variant in the extended defects possible for the rutile structure. Ga^{3+} and Fe^{3+} are similar in ionic radius to Cr^{3+} and Ti^{4+} (Ga^{3+} 0.062 nm, Fe^{3+} 0.064 nm, Cr^{3+} 0.063 nm, Ti^{4+} 0.068 nm) and smaller than Ti^{3+} (0.076 nm). All these trivalent cations form corundum-type oxides.

The gallium oxide–titanium oxide phase system has not been studied in detail. Lejus et al. (*13*) studied the phase Ga_2TiO_5 (pseudobrookite structure) and found that it was unstable below 1570°K, decomposing to form an unidentified phase X and Ga_2O_3. Below 1370°K only TiO_2 and Ga_2O_3 were found. They obtained rough values for the limits of phase X (Fig. 1) which they show to have a eutectoid. No further work has since been carried out on this phase X and until now the nature of this phase was not known.

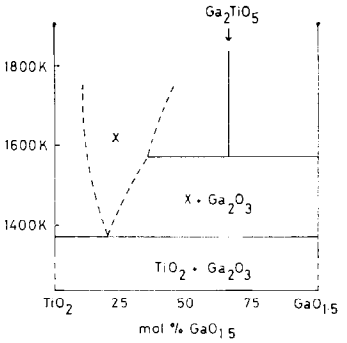

FIG. 1. TiO_2–Ga_2O_3 phase system after Lejus et al. (*13*).

The iron oxide–titanium oxide phase system is better documented. Karkhanavala and Momin (*14*) have determined the phase diagram by X-ray methods and found only one intermediate phase, pseudobrookite Fe_2TiO_5, which appears to be stable at all temperatures up to its melting point. No intermediate phases were detected at the high-titanium end of the system. The solid solubility of Fe_2O_3 in rutile has also been determined and has a value of 2.5 mole% $FeO_{1.5}$ at 1470°K (*15*).

Experimental

Several sample compositions in the TiO_2–Ga_2O_3 and TiO_2–Fe_2O_3 systems were prepared with compositions between 2.0 and 32.0 at.% $MO_{1.5}$. All samples were prepared directly from "Specpure" oxides by a solid state reaction in air at 1570°K. The reagents were mixed, finely powdered and pressed into a pellet before the annealing process. The pellet was laid on a thin sheet of platinum in an alumina boat to prevent contamination. All samples were annealed for 14 days.

X-Ray powder diffraction patterns were taken from each sample using a Guinier–Hägg camera to identify the products.

The quenched samples were microcrystalline and ranged in colour from pale brown for those low in dopant, to white for those with high gallium content. The samples were prepared for microscopy by crushing between glass slides and depositing the fragments on carbon-coated grids.

The electron microscopy was carried out with a JEM 6A fitted with a stage giving a tilt of $\pm 20°$ and a specimen rotation of 360°, and with a JEM 100U fitted with a small angle tilting stage of $\pm 10°$ in any direction. The JEM 100U could also be used for high resolution dark field microscopy by using the electrostatic beam deflectors; this was the preferred procedure for lattice imaging.

Results

2 mole% $MO_{1.5}$. At this composition the gallium and the iron doped systems gave identical results by electron microscopy. X-Ray powder diffraction patterns showed only rutile reflections and this composition therefore falls within a rutile solid solution range for both systems.

Transmission electron microscopy revealed large numbers of planar boundaries on more than one crystallographic orientation. In general, these boundaries terminated only at the edge of the crystal, but some were observed to terminate within the fragment, either on meeting another fault or at a dislocation.

By carefully tilting the specimen to bring the plane of the boundary parallel to the electron beam it was seen that they lay along the {210} rutile. The electron diffraction pattern was streaked perpendicular to the fault. Figure 2 shows planar boundaries along all four possible {210} boundaries, in dark field, the beam having been tilted slightly away from the optimum positions in order to bring out the contrast of the boundaries. The angles between the boundaries agree with those computed for the angles between rutile {210} planes.

Close observation of the fringes shows that fringe contrast is symmetrical both in bright field and in dark field. The boundaries are therefore of π type, with the characteristics of α boundaries (as defined by van Landuyt et al.) across which the structure is displaced by a vector **R**. The fringe contrast was analysed using bright field and dark field microscopy under two-beam conditions, and fringe profiles were computed for different values of α, crystal thickness, extinction distance and the excitation error s. The observed and computed profiles were compared in order to obtain the best fit, and a value of α could thereby be assigned to each fringe pattern. The displacement vector **R** could then be obtained from a number of these assignments, through the relation

$$\alpha = 2\pi \mathbf{g} \cdot \mathbf{R}$$

where **g** is the reciprocal lattice vector of the excited reflection.

It has been found that the Ga_2O_3–TiO_2 and Fe_2O_3–TiO_2 systems are only two of several

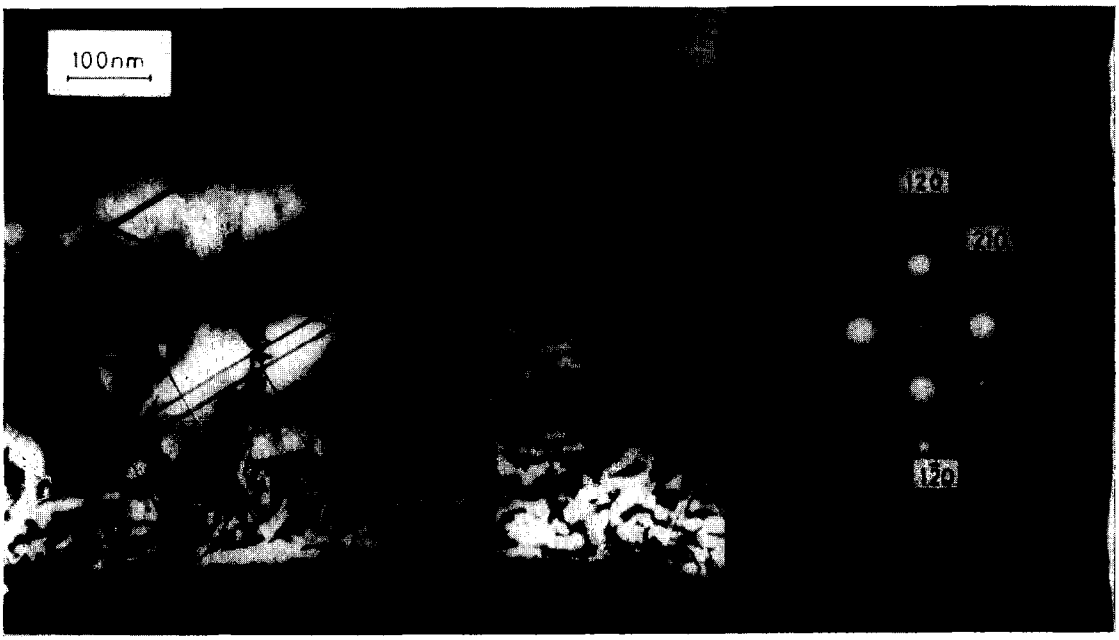

FIG. 2. An 001 section showing isolated boundaries of all four possible {210} orientations in TiO_2 2% $FeO_{1.5}$.

ternary rutile-based systems that present {210} boundaries, and the analysis of the fault will be more fully discussed elsewhere, in relation to a wider range of evidence. For present purposes, the observations can be summarized:

(1) For the 200, 020 and 002 reflections, fringe contrast was zero, or close to zero;
(2) No boundary was seen in contrast for both the 101 and 011 type reflections;
(3) A boundary in contrast for *hkl* is out of contrast for $2h$, $2k$, $2l$;
(4) 111 type reflections always gave π-type contrast. This critical observation is shown in Fig. 3 and confirmed by the zero contrast observed at two overlapping faults at A. The total phase change for overlapping faults is assumed to be twice that for a single fault where the interfault distance is small; thus at A the expected contrast would be for $\alpha = 2\pi$, consistent with the observation. Figure 4 shows contrast at two faults for differing diffracting conditions.

More strictly considered, the out of contrast condition did not correspond to exactly zero fringe contrast. It is clear that the condition $\alpha = 2n\pi$ can be attained only if **R** is a perfect lattice vector; in practice, any collapse process that rearranges the linkages of the $[MO_6]$ coordination polyhedra is likely to involve a certain measure of distortion, with the consequence that **R** may differ to some extent from the ideal value. Thus, in their careful analysis of {132} boundaries in oxygen-deficient rutile, Bursill and Hyde found that fringe contrast was best accounted for on the basis that **R** is about 0.90 times a perfect lattice vector. Comparison of their published out-of-contrast fringe images with those obtained by us suggests that **R** for {210} boundaries is rather closer to, but not exactly, a perfect lattice vector.

In Table I, the observed contrast under two-beam conditions is compared with that predicted for α boundaries with several different displacement vectors. It is apparent that the only values of **R** consistent with the observed contrast are $\frac{1}{2}[0,1,0]$ and $\frac{1}{2}[0,-1,0]$. Since a displacement vector $\frac{1}{2}[0,-1,0]$ would represent an expansive displacement, i.e., an increase in the oxygen: metal ratio, it is ruled out by the chemistry of the system. The first three displacement vectors in Table I are those that might be predicted on purely crystallographic grounds as compatible with a true α boundary. $\frac{1}{2}[121]$ corresponds to a

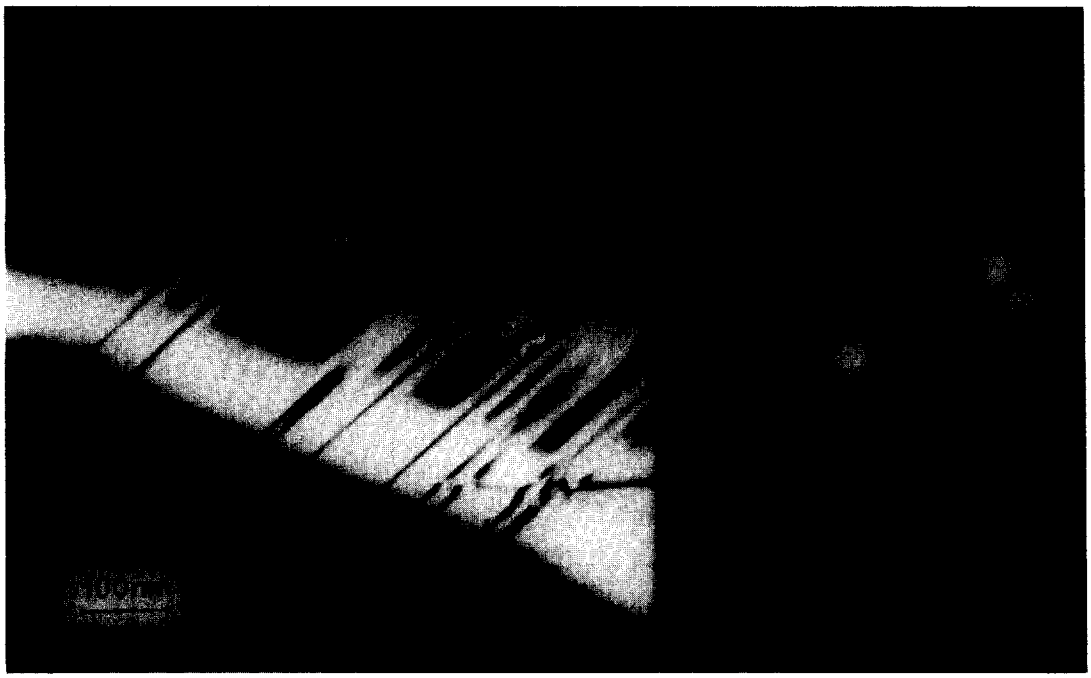

FIG. 3. π contrast for planar boundaries in dark field using the 111 reflection. Note the zero contrast at the two overlapping faults at A.

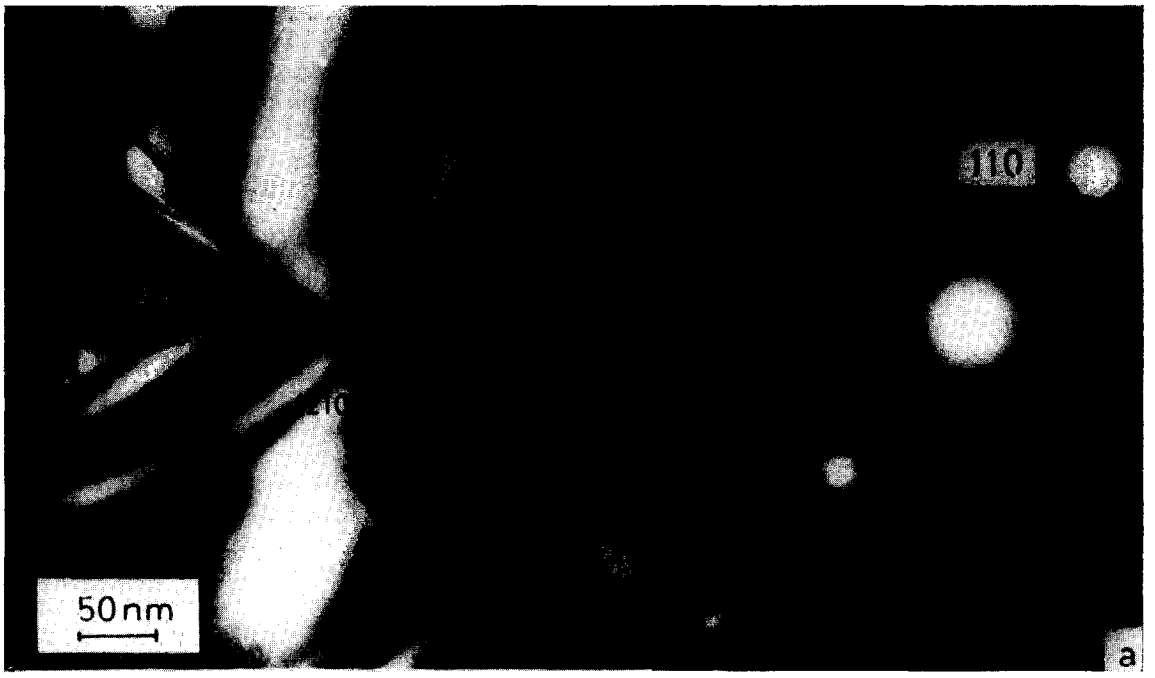

FIG. 4a.

stacking fault with no nett change in oxygen: metal ratio. $\frac{1}{2}[011]$ is a collapsing shear displacement, in harmony with the reduction in oxygen: metal ratio. A crystallographic shear with displacement vector $\frac{1}{2}[101]$ (as in the known {211} rutile shear) is less likely, since, operating on {210}, it would lead to three face-sharing octahedra along the [010] direction. However,

FIG. 4b.

FIG. 4c.

all these displacements with a component along c are eliminated by the observed π contrast for $\mathbf{g} = 111$.

The conclusion that the displacement vector is $\mathbf{R} = \frac{1}{2}\langle 0,b,0\rangle$ operating on $\{210\}$ creates a problem, however. A lattice vector $\frac{1}{2}[010]$ would bring titanium atoms into a set of octahedral sites, but it does not bring the oxygen sites of the rutile

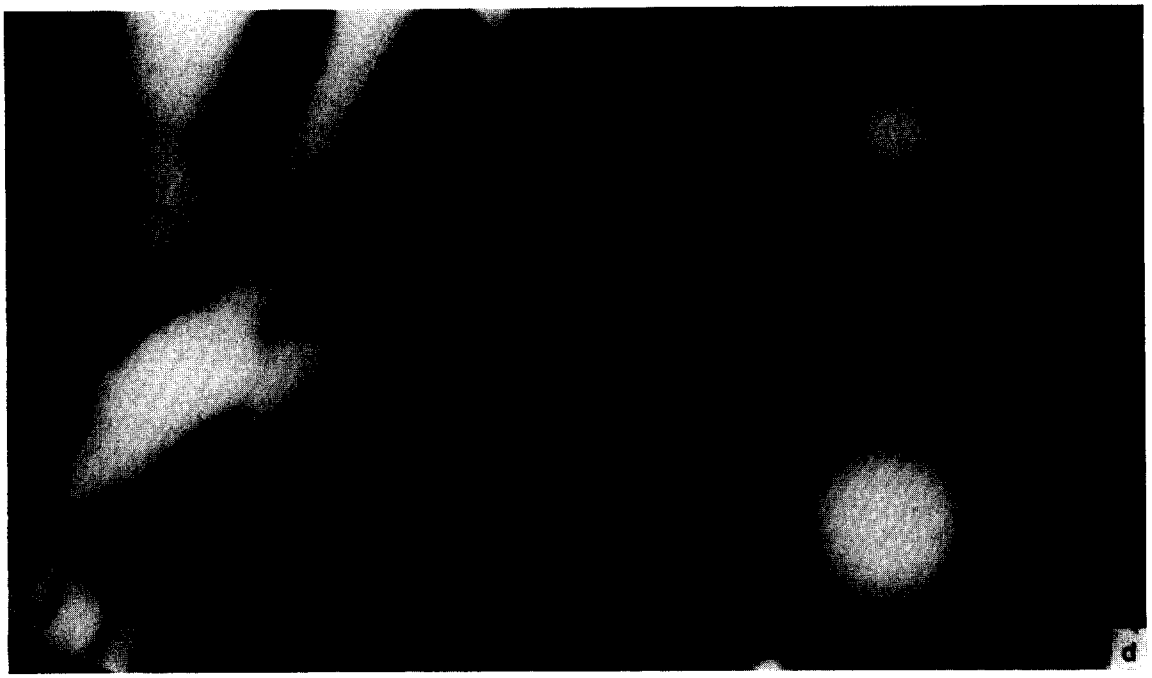

FIG. 4d.

FIG. 4e.

FIG. 4. Dark field images of faults on the (210) and (120) planes using (a) 110, (b) 101, (c) $01\bar{1}$, (d) $12\bar{1}$ and (3) $00\bar{2}$ reflections.

structure into coincidence; only the displacement vectors with a component $\pm\frac{1}{2}c$ do this. To translate unaltered rutile structure, across the boundary, by $\frac{1}{2}[0,b,0]$—as is required for a true α boundary—would involve a complete rearrangement of oxygen positions and reconstruction of coordination octahedra in the boundary itself. On purely structural grounds it can be argued that displacement of the titanium atoms alone by $\frac{1}{2}[0,b,0]$, within an unchanged oxygen sublattice, would give a rational structure at the boundary. However, the relation between the two blocks of rutile separated by the {210} interface would not then be defined by a simple translation; the boundary would not be strictly defined as an α boundary and it is not clear whether the contrast properties, and the inferences to be drawn from them, would be as set out above. We have, however, adopted this working hypothesis in a tentative way in discussing the homologous series of compounds in the Ga_2O_3–TiO_2 system (below). In our view, the structure of the {210} boundaries can be properly resolved only by a crystal structure determination of one of these phases.

TABLE I

PREDICTED CONTRASTS FOR POSSIBLE DISPLACEMENT VECTORS UNDER GIVEN REFLECTIONS COMPARED WITH THOSE OBSERVED

$\bar{g}$	110	101	$01\bar{1}$	$12\bar{1}$	$2\bar{1}1$	002	200	111
$\frac{1}{2}[121]$	3π	2π	π	4π	π	2π	2π	4π
$\frac{1}{2}[001]$	π	π	0	π	0	2π	2π	2π
$\frac{1}{2}[101]$	π	2π	$-\pi$	0	3π	2π	2π	2π
$\frac{1}{2}[010]$	π	0	π	2π	$-\pi$	0	0	π
obs	π	0	π	0	π	0	0	π

2.0–32.0 at.% $FeO_{1.5}$. For samples made up with iron content in excess of the rutile solid solution limit, the X-ray powder diffraction patterns gave two sets of lines, all of which could be indexed on the basis of either rutile or pseudobrookite (Fe_2TiO_5). No extra lines were observed.

These two phases were also observed by electron diffraction. Electron diffraction contrast also showed fragments of rutile containing large numbers of {210} faults. The existence of a two phase region containing rutile solid and Fe_2TiO_5, as observed by X-ray analysis in this composition range, is thus confirmed by electron diffraction.

2.0–32.0 at.% $GaO_{1.5}$. X-Ray diffraction patterns of samples in this composition range each contained a large number of lines. A few of the lines could be indexed on the basis of rutile.

By electron diffraction, single crystal fragments gave rutile reciprocal lattice sections but in many cases they contained superlattice spots. The shortest reciprocal lattice spacings were found along the $\langle 210 \rangle$ direction, often as heavy streaking or as several superimposed arrays. Bright and dark field imaging showed large variations in fringe spacing (Fig. 5).

At higher gallium contents it was possible to observe diffraction patterns with just one or two different superlattice spacings. Direct lattice imaging showed that the fringes were well ordered over short distances but anomalies in spacing were still frequent (Fig. 6).

The superlattice spots always appeared to intersect the [210] direction by an integral number of times, defined below as $n = (m - 1)/2$. Table II shows the observed spacings for various values of n. Diffraction patterns with higher values of n were observed but these were accompanied by streaking so that accurate spacings could not be obtained.

No streaking of the superlattice in other directions was observed in any specimen. It was always found that the $[\bar{1}10]$ was divided into three, $[\bar{2}10]$ into four and the $[\bar{3}10]$ into five equal parts (Fig. 7a, b), as required by a superlattice along $[\bar{2}10]$.

All the above facts point to the existence of a series of ordered phases based on the {210} fault described earlier. These boundaries are aligned and regularly recurrent, thus defining the individual members of a homologous series. The analogy with the homologous shear structure oxides is close.

Discussion

The observations reported above show clearly the existence of a new type of planar boundary occurring in rutile structures, defined by the fault plane {210} and, perhaps with less certainty, by the displacement vector $\frac{1}{2}\langle 0, b, 0 \rangle$. As with the crystallographic shear planes, this constitutes an

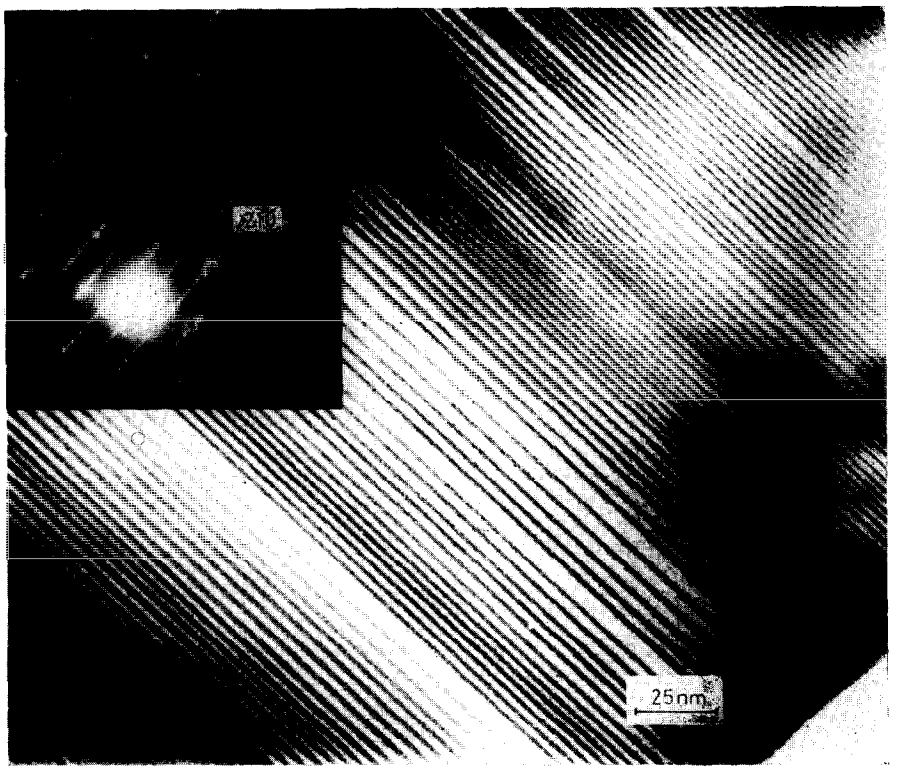

FIG. 5. Direct lattice images of variables spacing in fringes in material containing ~12% $GaO_{1.5}$.

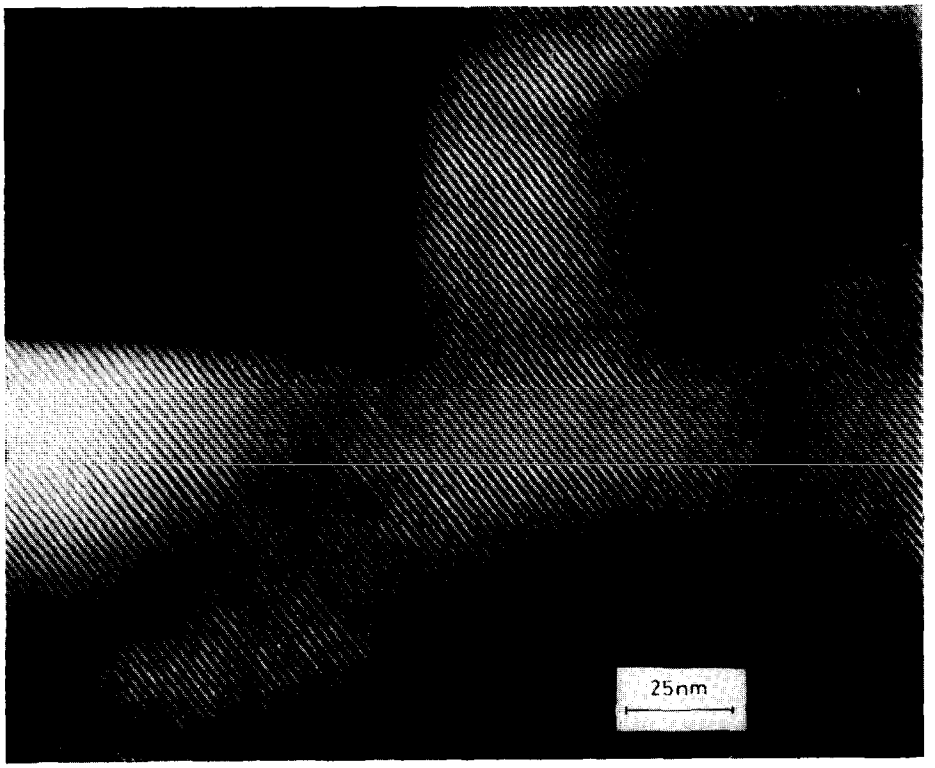

FIG. 6. Dark field lattice images from $Ga_4Ti_{13}O_{32}$ showing regions of well ordered material.

extended defect in rutile solid solutions and a means of generating a homologous series of compounds. The structure we propose for this fault is given in Fig. 8 and corresponds to an unaltered oxygen lattice with the displacement applied to the metal lattice only, so that the filled octahedra are now face sharing along the fault plane. The displacement vector assigned does not correspond to any mechanism for the formation of the fault, but indicates the relationship between the atomic positions on either side of the fault.

TABLE II

FAULT SPACING FOR NUMBERS OF THE HOMOLOGOUS SERIES $Ga_4Ti_{n-4}O_{2n-2}$

$(m-1)/2$	D (nm)	$[(m-1)/2]d_{210}$ (nm)
7	1.46 0.03	1.44
8	1.67 0.03	1.64
9	1.87 0.03	1.85
10	2.09 0.03	2.05
11	2.25 0.03	2.26
	2.27 0.05	

By considering the stacking sequence of (210) planes on either side of the fault, it will be seen that the number of metal atoms is doubled along the fault plane. In the idealized structure the stacking would be as follows:

$M, O_2, M, O_2, M, O_2 \ldots M, O_2, M_2, O_2, M, O_2.$

The fault corresponds to a lamella of structure with the formula M_3O_5.

This faulting therefore leads to a new manner in which rutile can assimilate a deficiency of oxygen without any defects of local order. The planar boundary is not readily described in crystallographic terms. It is not exactly a shear plane of the kind envisaged by Wadsley, since it cannot be derived from the rutile structure by a nonconservative shear. It will be noted that the displacement of cations from "normal" to octahedral "interstitial" sites at the same level reverses the obliquity of the ribbons of edge sharing octahedra running along the c axis, so that in each lamella enclosed between successive fault planes they are in a mirror image relation to those of adjacent lamellae. (210) is not a twin plane for rutile; the reversal of sense is nonconservative. There is a structural similarity to

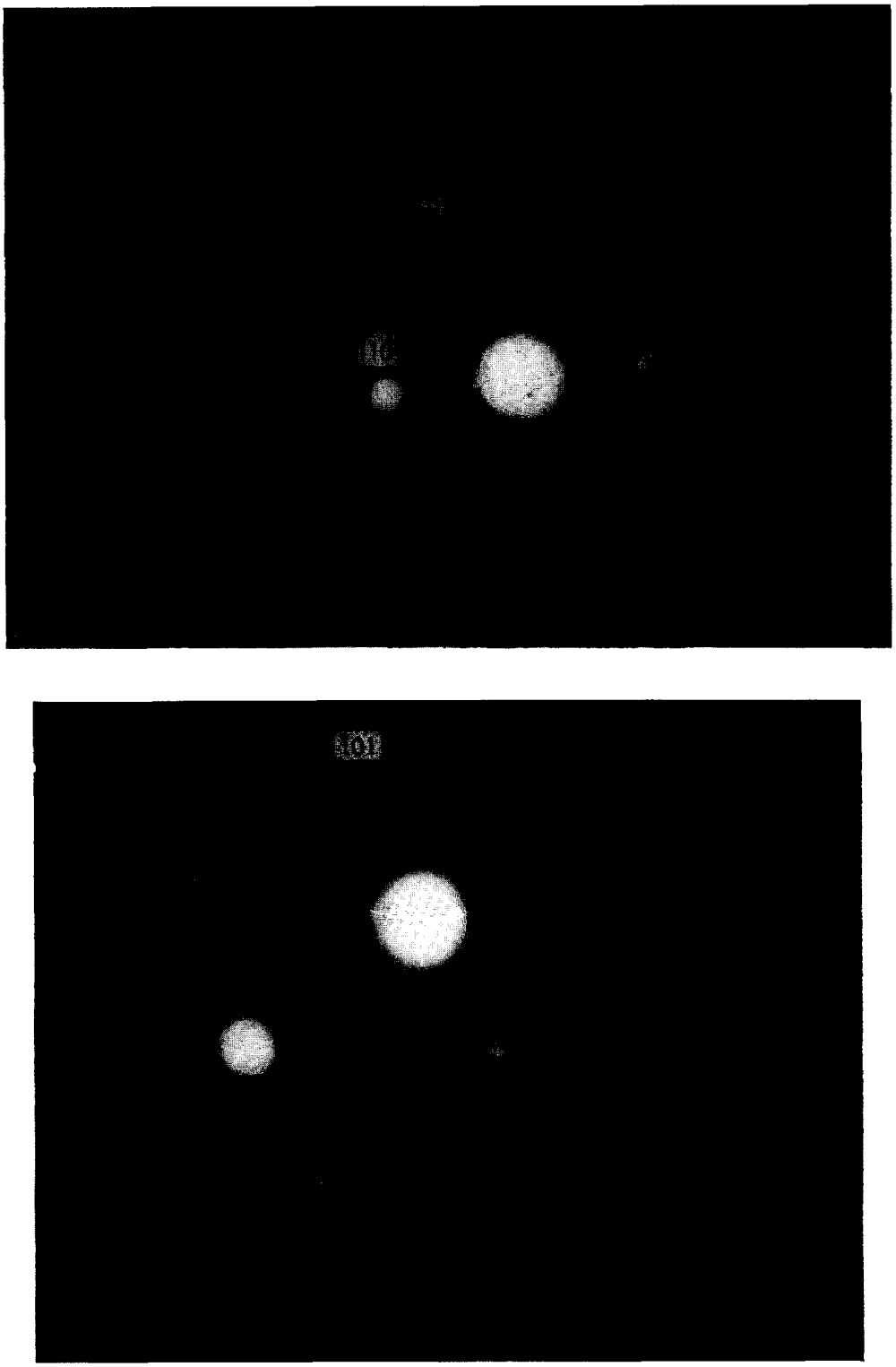

FIG. 7. Diffraction patterns from ordered material showing (a) the [110] divided into three and (b) the [310] divided into five equal parts by superlattice spots.

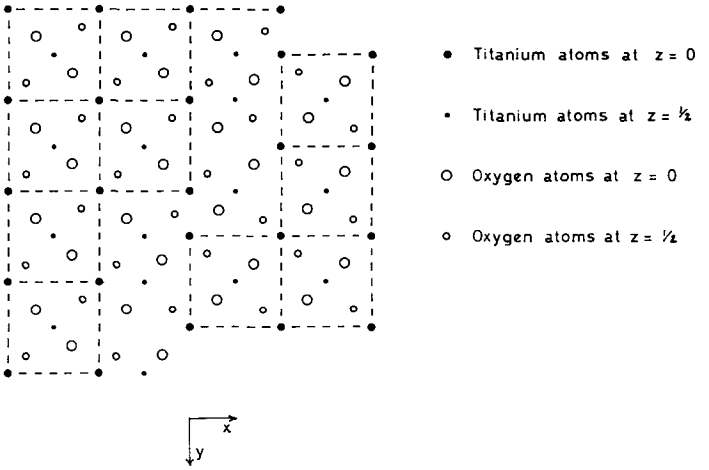

FIG. 8. Atomic positions in the idealized structure across a {210} boundary.

{121} crystallographic shear in that, at any one level, the arrangement of face sharing octahedra at the fault plane is identical; in the proposed (210) boundary, however, ribbons of face-sharing octahedra run parallel to [001] rutile: In one sense, the (210) fault could be considered as arising from {121} shear operating alternately on $(12\bar{1})$ and (121) at each successive layer. This may be significant, but the similarity must not be pressed too far. Nevertheless, both types of fault correspond to modes of lowering the oxygen: metal ratio by forming boundaries across which "normal" and "interstitial" cation sites interchange their meaning.

This type of boundary cannot be formed by the vacancy loop mechanism put forward by Anderson and Hyde (*16*), since this includes a shear process in forming the collapsed vacancy disc. However, the mechanism of Andersson and Wadsley (*17*) is pertinent, since it involves a jump of titanium atoms, in either the [100] or the [010] direction, into vacant interstitial positions. It will be noted that such a process is suggested by the calculated displacement vector of $\frac{1}{2}\langle 0,1,0\rangle$. Unfortunately, it is not possible, in synthesizing ternary compounds, to observe the formation and growth of the faults, as Anderson and Tilley (*5*) could in reduced rutile.

Regularly recurrent boundaries generate a new series of ordered phases $Ga_4Ti_{m-4}O_{2m-2}$ in the gallium oxide–titanium oxide system, based on the rutile unit cell as a subcell. Only those members with odd values of m can exist, and these are generated by boundaries of the type shown at every $(m-1)/2$ (210) planes. Calculated values of $[(m-1)/2]d_{210}$ are compared with the observed spacings in Table II. The unit cell proposed for these compounds can be defined as follows, where the subscript r denotes the rutile axes.

For $\frac{m-1}{2}$ even

$$a = c_r$$
$$b = -a_r + 2b_r$$
$$c = \frac{(m-3)}{4} a_r + b_r + c_r/2$$

For $\frac{m-1}{2}$ odd

$$a = c_r$$
$$b = -a_r + 2b_r$$
$$c = \frac{(m-1)}{4} a_r + c_r/2.$$

Indices of planes can be converted from rutile to the new unit cell by means of the transformation matrices

rutile

$$\begin{array}{|ccc|} 0 & 0 & 1 \\ -1 & 2 & 0 \\ \frac{m-3}{4} & 1 & \frac{1}{2} \end{array} \quad \text{for } \frac{m-1}{2} \text{ even}$$

rutile

$$\begin{array}{|ccc|} 0 & 0 & 1 \\ -1 & 2 & 0 \\ \frac{m-1}{4} & 0 & \frac{1}{2} \end{array} \quad \text{for } \frac{m-1}{2} \text{ odd}$$

Solving for a_r, b_r, and c_r when $(m-1)/2$ is even

$$a_r = -\frac{2a}{m-1} - \frac{2b}{m-1} + \frac{4c}{m-1}$$

$$b_r = -\frac{a}{m-1} + \frac{(m-3)b}{2(m-1)} + \frac{2c}{m-1}$$

$$c_r = a$$

when $\frac{m-1}{2}$ is odd

$$a_r = -\frac{2a}{m-1} + \frac{4c}{m-1}$$

$$b_r = \frac{-a}{m-1} + \frac{b}{2(m-1)} + \frac{2c}{m-1}$$

$$c_r = a.$$

These equations lead to the inverse matrices for converting atomic positions based on the rutile cell to those on the new unit cell.

For $\frac{m-1}{2}$ even

	$\frac{-2}{m-1}$	$\frac{-2}{m-1}$	$\frac{4}{m-1}$
rutile	$\frac{-1}{m-1}$	$\frac{(m-3)}{2(m-1)}$	$\frac{2}{m-1}$
	1	0	0

	$\frac{-2}{m-1}$	0	$\frac{4}{m-1}$
	$\frac{-1}{m-1}$	$\frac{1}{2(m-1)}$	$\frac{2}{m-1}$
rutile	1	0	0

The relationship between the unit cell for $(m-1)/2 = 10$ and rutile containing regular {210} planar boundaries is shown in Fig. 9.

Several preparative methods have been unsuccessfully tried in order to produce homogeneous single crystals for crystal structure determinations. Chemical vapour transport, with $TeCl_4$ as transport agent, does produce small crystals, but it will be necessary to establish that these are completely homogeneous before a structure determination can be made. The structure proposed is therefore based only on the electron diffraction data, cell dimensions and structural principles applicable to the assigned displacement vector.

These observations explain the puzzling phase

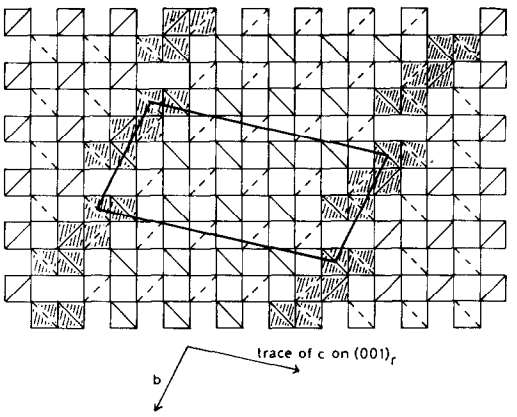

FIG. 9. The unit cell of $Ga_4Ti_{17}O_{40}$ related to the ordering of (210) faults.

X observed by Lejus et al. The forces of ordering in these phases are apparently not as great as those observed in the reduced rutile system even at high gallium content; this is probably why it has proved difficult to grow single crystals. The disorder is brought out by direct lattice imaging, which shows that not only does the spacing vary slightly from fringe to fringe, but it is also possible to observe isolated spacings as large as 5 nm in material with low gallium content. The lower limit of the phase range, as given by Lejus, can be ignored since undoubtedly there is a gradual transition from isolated {210} faults towards ordering.

At high gallium content there is much better ordering, and regularly spaced fringes are observed over quite large areas. The highest member of the series observed at 1570°K was $m = 15$, as against $m = 11$ estimated from the Lejus phase diagram. However, a sample annealed at 1370°K showed a mixture of $m = 19$ and 21, in agreement with Lejus.

Two points concerning the electron diffraction patterns must be discussed. Firstly, we have identified each phase by the number of (210) planes between each fault, which is given by counting the number of superlattice spots between the undiffracted beam and the first strong reflection. Figure 10a shows a ten times superlattice where $m = 21$. However, on the first layer line there are 21 spots between the two strong reflections and no single strong spot occurs between them. Figure 10b shows this schematically and the superlattice reflections have been indexed. The position of the disallowed 001 rutile reflection lies at 1, 0, $\frac{1}{2}$ as calculated from the

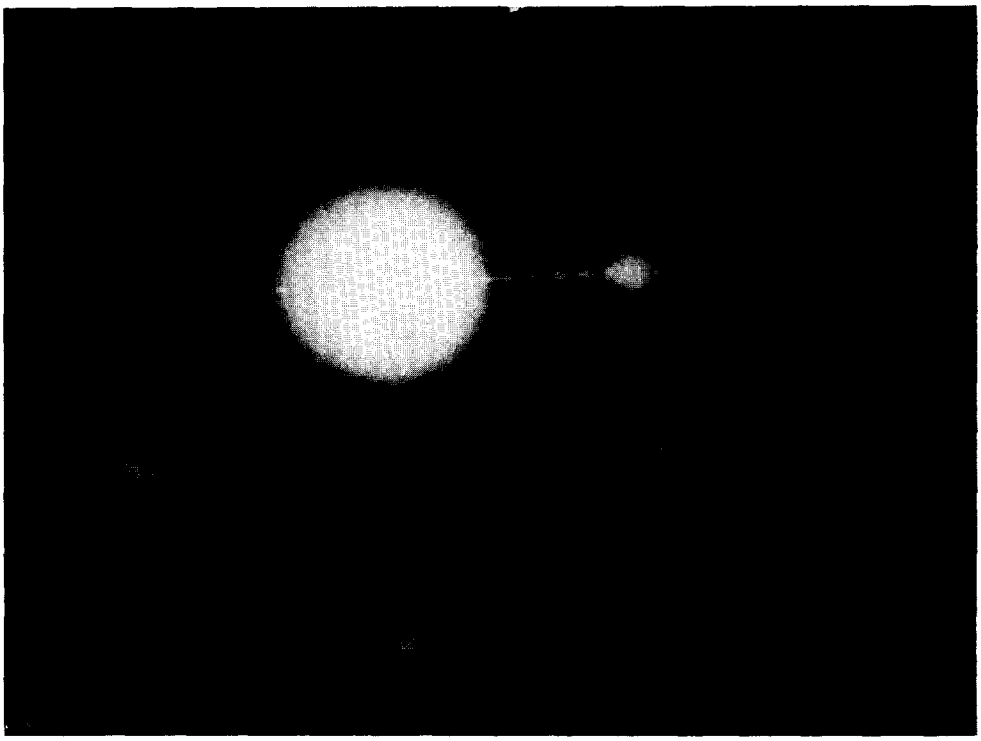

FIG. 10. (a) Diffraction pattern from material in which $(m-1)/2 = 10$.

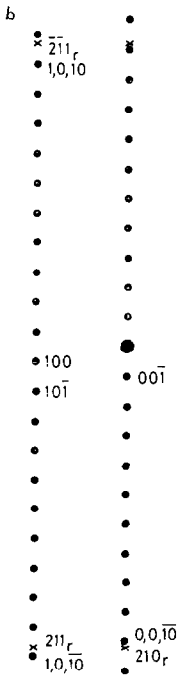

FIG. 10. (b) Schematic representation of the diffraction pattern assuming a slight expansion at the fault plane.

transformation matrix, between the 100 and 101 superlattice spots. If we now assume that the (001) spacing of the superstructure is slightly larger than 10 times d_{210}, as would be expected if a slight expansion occurs at the fault plane compared with that predicted by the displacement vector, then the 210 rutile reflection (marked by a cross) does not coincide with the 0, 0, $\bar{1}\bar{0}$ spot. However, the intensity of the 0, 0, $\bar{1}\bar{0}$ reflection is increased by its close proximity. When the second layer line reflections are drawn and the rutile reflections added, additional intensity will occur for the 1, 0, $\bar{1}\bar{0}$ and 1, 0, $\bar{1}\bar{1}$ reflections, and there are 21 superlattice spots between these two intense reflections. We should, therefore, predict that for an $(m-1)/2$ times superlattice the interplanar spacing derived from the diffraction pattern would be larger than that calculated from the simple formula $[(m-1)/2]d_{210}$. Table II shows this to be correct. Experimental errors in measuring the superlattice spacing prevent us from determining the expansion at the fault, but this is probably small, since isolated faults do not deviate significantly from the contrast predicted for a displacement vector of $\frac{1}{2}\langle 010\rangle$.

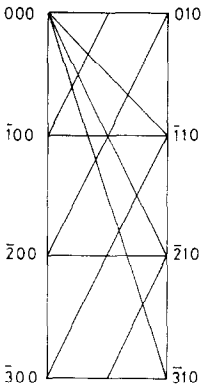

FIG. 11. Rutile 001 reciprocal lattice section.

A second observation meriting comment is that, for all phases, superlattice spots occur along the $[\bar{1}10]$, $[\bar{2}10]$, and $[\bar{3}10]$ directions, dividing these into 3, 4 and 5 equal distances respectively. By using the transformation matrices it may be seen that these rutile planes do not necessarily correspond directly to low index planes in the superstructure cell. Figure 11 shows a section of the rutile 001 reciprocal lattice plane, with the [210] superlattice direction marked by diagonal lines. $[\bar{1}10]$ cuts these superlattice directions twice $[\bar{2}10]$ three times and $[\bar{3}10]$ four times. Superlattice spots will thus appear at $\frac{1}{3}[\bar{1}10]$ etc. providing superlattice points occur at the intersections of these lines in reciprocal space. Even though superlattice points may not occur at these intersections, there are two ways in which diffraction spots can be observed. Firstly the superlattice is often highly streaked due to the disorder in fault plane spacing. If such a streaking is intersected, a superlattice spot will be observed. The second, and probably the more important effect is that, for a thin crystal, reciprocal lattice points become spikes in a direction normal to the crystal face. For a thin crystal lying normal to the beam, these spikes will also be normal to the Ewald sphere, and points slightly below and above the Ewald sphere will show up on the diffraction pattern even though they do not lie exactly on the reciprocal lattice section.

It is clear from this work that different cations, of similar charge and ionic radius, as dopants or as significant ternary components, can exercise quite different influences on the defect structure of rutile. There is, as yet, too little evidence to advance any interpretation of this specificity.

References

1. S. ANDERSSON, *Acta Chem. Scand.* **14**, 1161 (1960).
2. S. ANDERSSON, B. COLLEN, U. KUYLENSTIERNA, AND A. MAGNÉLI, *Acta Chem. Scand.* **11**, 1641 (1957).
3. S. ANDERSSON AND L. JAHNBERG, *Ark. Kemi* **22**, 413 (1963).
4. S. ANDERSSON, B. COLLEN, G. KRUUSE, W. KUYLENSTIERNA, A. MAGNÉLI, H. PESTMALIS, AND S. ASBRINK, *Acta Chem. Scand.* **11**, 1653 (1957).
5. J. S. ANDERSON AND R. J. D. TILLEY, *J. Solid State Chem.* **2**, 472 (1971).
6. L. A. BURSILL, B. G. HYDE, O. TERASAKI AND D. WATANABE, *Phil. Mag.* **20**, 347 (1969).
7. O. TERASAKI AND D. WATANABE, *Jap. J. Appl. Phys.* **10**, 292 (1971).
8. L. A. BURSILL AND B. G. HYDE, *Proc. Roy. Soc. A* **320**, 147 (1970).
9. L. A. BURSILL AND B. G. HYDE, *Acta Crystallogr.* **27**, 210 (1971).
10. S. ANDERSSON, A. SUNDHOLM, AND A. MAGNÉLI, *Acta Chem. Scand.* **13**, 989 (1959).
11. R. M. GIBB AND J. S. ANDERSON, *J. Solid State Chem.* **4**, 379 (1972).
12. L. A. BURSILL, B. G. HYDE, AND D. K. PHILP, *Phil. Mag.* **23**, 1501 (1971).
13. A. LEJUS, D. GOLDBERG, AND A. REVCOLEVSCHI, *C.R. Acad. Sci.* **263C**, 1223 (1966).
14. M. D. KARKHANAVALA AND A. C. MOMIN, *J. Amer. Ceram. Soc.* **42**, 399 (1959).
15. O. W. FLORKE AND G. W. LEE, *J. Solid State Chem.* **1**, 445 (1970).
16. J. S. ANDERSON AND B. G. HYDE, *J. Phys. Chem. Solids* **28**, 1393 (1967).
17. S. ANDERSSON AND A. D. WADSLEY, *Nature (London)* **211**, 581 (1966).